J Mater Sci (2013) 48:7974–7980
DOI 10.1007/s10853-013-7608-y

Effect of starting PMMA content on microstructure and properties of gel casting BN/Si_3N_4 ceramics with spherical-shaped pore structures

Shengjin Wang · Dechang Jia · Wang Cui · Zhihua Yang · Xiaoming Duan · Yingfeng Shao · Yu Zhou

Received: 29 April 2013 / Accepted: 18 July 2013 / Published online: 27 July 2013

Abstract By gel casting with polymethylmethacrylate microbeads (PMMA) as pore-forming agent, porous boron nitride/silicon nitride (BN/Si_3N_4) composite ceramics were successfully prepared. The obtained ceramic shows bimodal hierarchical structures that composed of spherical-shaped micro pores depending on PMMA content and irregular sub-micro pores formed by the stacking of ceramic particles. Porosity of the porous BN/Si_3N_4 ceramics can be well controlled from 53.0 to 60.6 % by the PMMA content from 10 to 40 wt%, as well as the mechanical and dielectric properties. Effect of PMMA content on phase composition and the relationship between microstructure and the basic properties of the porous BN/Si_3N_4 ceramics was discussed in detail. Microstructure analysis reveals that the sub-micro pores acted as channels between micro pores. BN particles have a relatively denser distribution on the wall of spherical-shaped micro pores with a window between micro and sub-micro pores, and resulting in a half-closed micro pore structure, which is meaningful for material design with concentration of BN particles on the wall of pore structure.

S. Wang · D. Jia (✉) · W. Cui · Z. Yang · X. Duan · Y. Zhou
Institute for Advanced Ceramics, Harbin Institute of Technology, Harbin 150001, China
e-mail: wangshengjin@hit.edu.cn

Y. Shao
State Key Laboratory of Nonlinear Mechanics (LNM), Institute of Mechanics, Chinese Academy of Sciences, Beijing 100190, China

Introduction

Boron nitride/silicon nitride (BN/Si_3N_4) ceramics have been regarded as promising materials for wave-transparent applications. The BN addition in Si_3N_4 matrix led to excellent mechanical and dielectric properties, thermal shock resistance, and machinability of the composite ceramics [1–7]. It has been found that the properties of BN/Si_3N_4 composite combined the favorable mechanical properties of Si_3N_4 and dielectric properties, resistance to thermal shock, and machination of BN [2, 4]. The development of aircraft requires higher broadband electromagnetic transmission performance of the wave-transparent materials, and a certain content of porosity is necessary to maintain the material with relatively low dielectric loss and moderate strength [5].

Up until now, porous ceramics with a wide range of porosity have been readily fabricated by various processing routes such as partial sintering [8], adding pore-forming agent [9, 10], direct foaming method [11], freezing casting [5, 12], and gel casting [13, 14]. Among these methods, freezing casting can control the porosity by solid content precisely but the prepared materials show anisotropic properties [15]. For adding pore-forming agent method, starch and other organic particles are often used to prepare porous ceramics with controllable porosity [9, 16], but the pore structure is usually irregular. The irregularly shaped pores usually connected with each other to create many sharp edges, which can cause more reflections in the ceramics and low permeate flux through the samples and lead to an increasing in the dielectric constant, as well as intensify the stress concentration [17]. In order to avoiding sharp edges, direct foaming method was employed to fabricate separately distributed porous ceramics with closed spherical-shaped pore structure [10], but the

fabricated materials usually show high porosity and low strength. PMMA microbeads as pore-forming agent were used to prepare spherical-shaped porous ceramics with controlled porosity [18]. However, it is hard for to homogeneously disperse ceramic powders in the traditional drying process, especially for the mixture of ceramic powders and organic pore-forming agent.

We have been committed to the study of preparing porous Si_3N_4-based ceramics with uniform structure by gel casting process over the past years [4, 19]. Based on our previous study [4], 10 vol% BN/Si_3N_4 ceramic with an excellence overall performance was prepared, and in order to further improve the porosity of BN/Si_3N_4 ceramics, adding pore-forming agent method and gel casting process were combined in this study. Different content of PMMA microbeads (10 μm in diameter) varying from 10 to 40 wt% were used as pore-forming agent to control the porosity. This paper also focuses on the effect of PMMA content on microstructure, phase composition, and the relationship between microstructure and material properties of the porous BN/Si_3N_4 ceramics.

Experimental procedures

The starting powders were Si_3N_4 (α-phase >93 %, mean particle size 0.5 μm) and h-BN (purity = 99.5 %, mean particle size 0.5 μm), and Y_2O_3 and Al_2O_3 (Aldrich Chemicals, purity = 99.99 %, particle size 50 nm) were used as sintering additives. PMMA (Athanasy Technology Co., Ltd., Beijing) with the diameter of 10 μm was used as pore-forming agent. Designations and corresponding composition of the ceramics are shown in Table 1. Numbers in the designations represent the content of PMMA.

In a typical experiment, initially, precursor mixtures containing Si_3N_4, BN, Y_2O_3, Al_2O_3, and different amounts of PMMA were suspended in a premix solution, which had been prepared by dissolving 0.2 wt% polyacrylic acid (PAA), 0.5 wt% acrylamide (AM), and 0.1 wt% *N*,*N*′-Methylenebis acrylamide (MBAM) in deionized water, and hydrochloric and ammonia were used to adjust the pH value to 8.5. Solid content of the suspensions was fixed at 38 vol%, and the slurries were ball-milled with Si_3N_4 balls for 24 h in a plastic bottle. The resultant suspensions were degassed for ~3 min when an initiator (ammonium persulfate) and a catalyst (*N*,*N*,*N*′,*N*′-tetramethylethylenediamine) were added at the ratio of 5 wt% and 3 ml/L, respectively. Afterward, the slurries were poured into a stainless steel mold (58 mm in diameter and 8 mm in height), which were then allowed to set under ambient conditions till the completion of the gelling process. The solidified green bodies were demoulded and dried at room temperature under controlled humidity to avoid cracking and nonuniform shrinkage caused by rapid drying. After the samples were completely dried, organic matters were removed in a muffle furnace at 550 °C for 1 h in an air atmosphere with a heating rate of 1 °C/min. Then, the samples were placed in a graphite crucible in a powder bed with a composition of 50:50 vol% for BN:Si_3N_4 and sintered in a graphite furnace at 1750 °C for 1 h under 0.1 MPa N_2 atmosphere.

Densities were calculated according to the dimensions and weight of the samples, and porosity was determined by the Archimedes method using distilled water as a medium. Phase compositions were identified by X-ray diffraction (XRD, Rigaku, RINT-2000). Morphologies were observed by scanning electron microscopy (SEM, FEI, Quanta-200). Samples were machined into standard bar samples of 36 mm × 4 mm × 3 mm and edges were beveled for three-point bending strength test, which was conducted on a mechanical testing machine (Shimadzu, AG-Is50) with a span of 30 mm at a crosshead speed of 0.5 mm/min, and five specimens were tested to obtain the average strength values. The fracture toughness was measured by a single edge notched beam (SENB) technique, the samples sizes were 20 mm × 4 mm × 2 mm, with a notch of 2 mm in depth and 0.2 mm in width. The thermal expansion coefficient of the obtained ceramics was determined by the thermal expansion instrument (NETZSCH DIL 402C). For the measurements of dielectric properties, specimens with a size of Φ 18 mm × 1 mm were tested in the frequency range of 21–38 GHz at room temperature by RF impedance/material analyzer (Model 4291B, Agilent, USA).

Table 1 Compositions of the starting powder

Designations	Si_3N_4 (vol%)	BN (vol%)	Y_2O_3 (vol%)	Al_2O_3 (vol%)	PMMA diameter (μm)	PMMA (wt%)
P10	85	10	3.5	1.5	10	10
P20						20
P30						30
P40						40

Results and discussion

Density and phase component investigation

Table 2 shows the effect of PMMA content on sintering linear shrinkage, density, and porosity of the porous BN/Si_3N_4 ceramics. From these values, it is evident that the porosity is a sensitive function of the PMMA content in the initial suspension, when the PMMA content increased from 10 to 40 wt%, the porosity of samples after sintering increased from 53.0 to 60.6 %. We can found that a large variation in the amount of PMMA microbeads only result in a total porosity variation of about 7.6 %. As porosity is a combining result of green density and sintering shrinkage, the green density decreased with the increasing of PMMA content in the suspension, while a much higher shrinkage (from 9.8 to 11.5 %) for the samples containing a large amount of PMMA microbeads can account for such a limited increase in the total porosity.

The XRD patterns of porous BN/Si_3N_4 ceramics with different content of PMMA are shown in Fig. 1. It can be seen that α-Si_3N_4, β-Si_3N_4, and h-BN are the dominating phases of all the four samples, and Y_2O_3 or Al_2O_3 was not detected in the XRD patterns due to their low amounts. According to the XRD patterns, with the increasing of PMMA content in the initial suspension, the diffraction intensity of β-Si_3N_4 declined apparently while the diffraction intensity of α-Si_3N_4 enhanced. The reason can be well explained by the liquid phase sintering of Si_3N_4-based ceramics. During the sintering, the removal of PMMA would leave pores in situ in the ceramic bodies, and thus retard the formation of necks among particles and impede atomic transport for α- to β-Si_3N_4 transformation by solution–diffusion–precipitation process.

Microstructures of the porous BN/Si_3N_4 ceramics

The typical microstructure of the fractured porous BN/Si_3N_4 ceramics prepared with 10, 20, 30, and 40 wt% PMMA are shown in Fig. 2. After the burning-out and sintering process, the pore-forming agent (PMMA) was successfully removed and leaves pores with the same shape

Table 2 Sintering linear shrinkage, density, and porosity of BN/Si_3N_4 ceramics with different content of PMMA

Designations	Sintering linear shrinkage (%)	Density (g/cm^3)	Porosity (%)
P10	9.8	1.48	53.0
P20	11.1	1.40	55.4
P30	11.2	1.32	58.2
P40	11.5	1.24	60.6

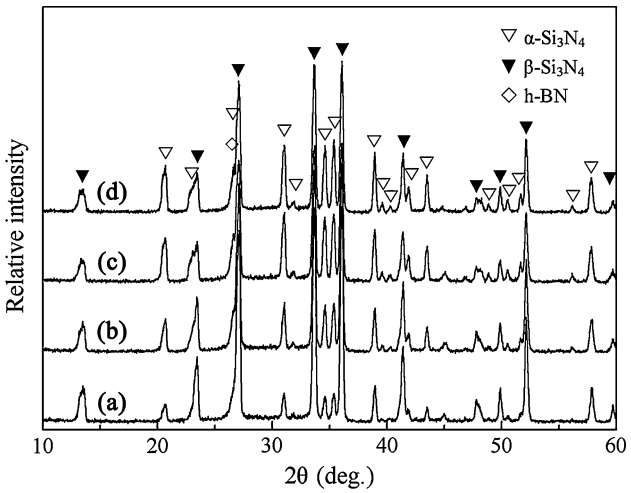

Fig. 1 XRD patterns of BN/Si_3N_4 ceramics with different content of PMMA: **a** P10, **b** P20, **c** P30, and **d** P40

of PMMA in situ. As can be seen, there are many spherical-shaped micro pores distributed uniformly in the continuous BN/Si_3N_4 matrix as the disperse phase, and no noticeable macro defects were detected. The phenomenon of pore "overlapping" was not found even in the sample P40 with the porosity as high as 60.6 %. This suggests that homogeneously distribution of ceramic powders and PMMA can be achieved through the way described in this study. As the PMMA content increased, the number density of pores significantly increased, as shown in Fig. 3a–d. This difference indicates that there is a high correlation between the initial PMMA content and the final porosity of the ceramics, so, the porous ceramics with similar morphologies but different porosities could be successfully prepared by this technique. Compared to previous studies [9, 18, 20] on porous ceramics with PMMA, starch, or other organic pore-forming agent, a great progress was achieved on the controllability of pore structure of high porosity porous ceramics with separately distributed pores, without "overlapping" micro pores.

Figure 3 shows the high magnification micrographs and EDS result of the obtained porous BN/Si_3N_4 ceramics. Figure 3a shows the high magnification micrograph of BN/Si_3N_4 ceramic. As can be seen, BN particles are homogeneously dispersed between Si_3N_4 grains, so the liquid diffusion rate and mass transport are retarded, and the growth of β-Si_3N_4 grain was restrained as a result. Thus, with the introduction of BN, the toughening effect of rod-like β-Si_3N_4 grain was restrained, in agreement with our previous study on porous BN/Si_3N_4 ceramics prepared by gel casting [4]. Besides, in addition to the spherical-shaped micro pores with the size of about 10 μm formed by burning-out of PMMA as shown in Fig. 2, other irregular sub-micro pores with the size of about 1 μm formed by

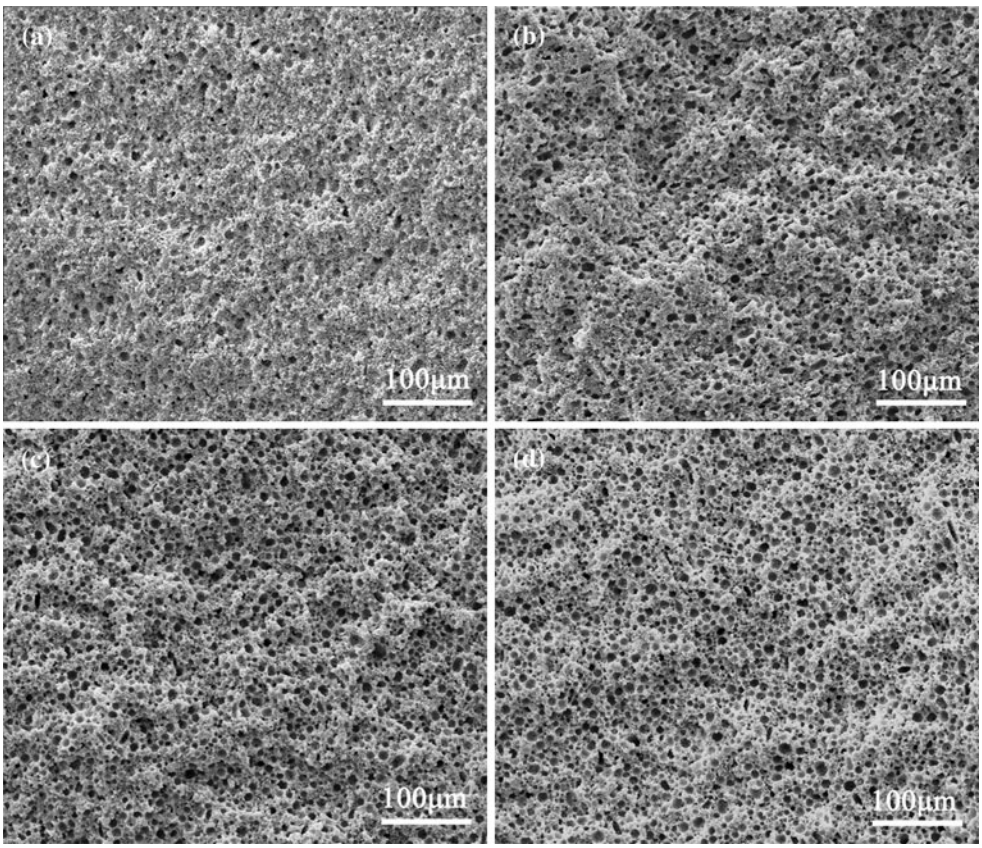

Fig. 2 SEM micrographs with low magnification of the porous BN/Si_3N_4 ceramics depending on the content of PMMA: **a** P10, **b** P20, **c** P30, and **d** P40

stacking ceramic powders are also detected in Fig. 3a. The sub-micro pore plays as the releasing channels for volatile matter during the burnout of green bodies.

Figure 3b shows the pore structures of 20 wt% PMMA content porous BN/Si_3N_4 ceramic. It was confirmed that the porous BN/Si_3N_4 ceramic has a bimodal hierarchical structure composed of spherical-shaped micro and sub-micro pores and the latter acted as channels between micro pores.

Furthermore, one point is worth mentioning: the micro pore with a relative denser wall was found, and the pore structure on the wall of micro pore plays a window between micro and sub-micro pores. In the enlarged spherical-shaped pore region (c), which obtained from the rectangular area of (b), many fine grains with a relative dense arrangement were clearly observed, and the growth of β-Si_3N_4 grain into the micro pore was restrained although there is enough space for it. In order to determine the composition of the densely arranged materials, area-scanning composition analysis was conducted at the rectangular area of (c), and the results are shown in (d). The elements in this region are mainly B and N with minor Si. The results show that the matter aggregated on the wall of spherical-shaped micro pore is BN particle, which indicated that PMMA may has a great adsorption effect on BN particles during the preparation of suspension. This is an interesting phenomenon, and has a significant guidance for material design with the concentration of BN particles on the wall of pore structure. Especially for fabricating porous BN/Si_3N_4 ceramics with densely wall structure to clear the relationship between the pore size and mechanical and dielectric properties. For the influencing factors and adsorption mechanism of PMMA on BN particles, we would conduct an overall investigation and to report in other studies.

Mechanical and thermal shock resistance of the porous BN/Si_3N_4 ceramics

Generally, the flexural strength of porous ceramics is mainly dependent on the porosity although the spherical-shaped pore structures can partly alleviate the stress concentration and contributed to the mechanical properties of the ceramics defined by the following equation [21]:

$$\sigma = \sigma_0 \exp(-nP), \quad (1)$$

where σ_0 is the flexural strength when the total porosity P is 0, n is the structural factor. The change of flexural strength and fracture toughness for all the samples as a function of PMMA content are shown in Fig. 4. As

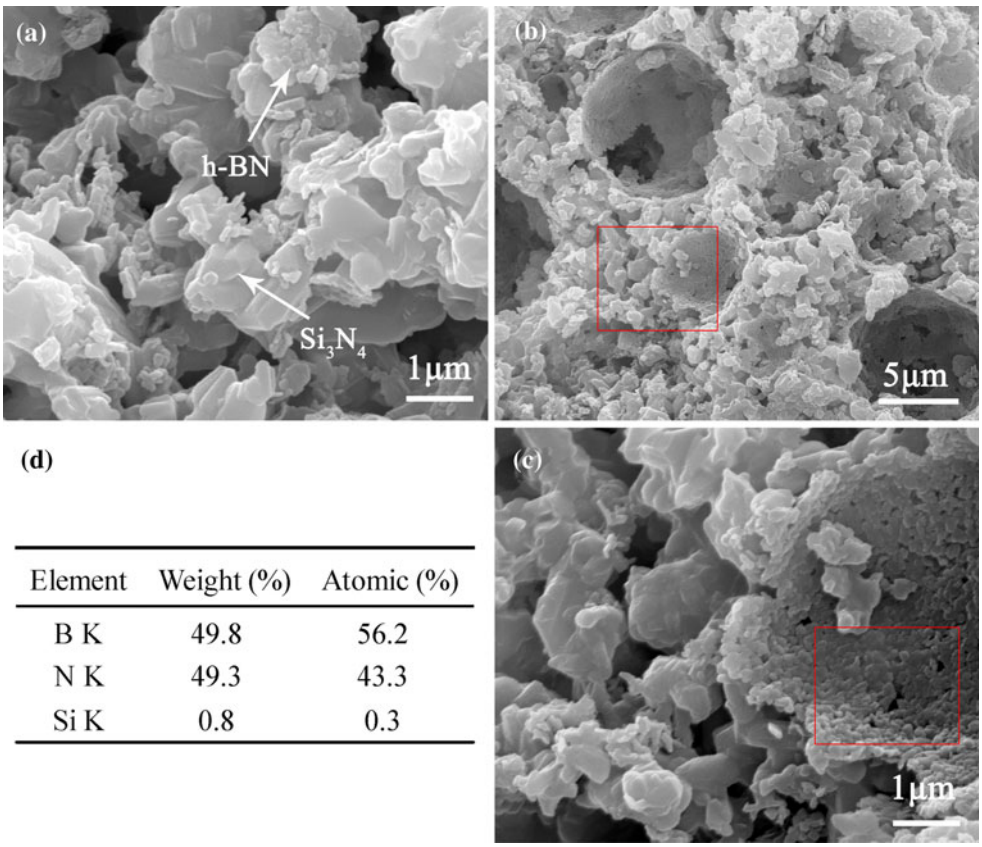

Fig. 3 SEM micrographs and EDS of the porous BN/Si_3N_4 ceramics: **a** shows the distribution of BN between Si_3N_4 grains, **b** shows the microstructure of *spherical-shaped pore* structure, **c** high magnification shows the *rectangular area* get from (**b**), and **d** EDS results of B, N, and Si get from the *rectangular area* of (**c**)

(d)

Element	Weight (%)	Atomic (%)
B K	49.8	56.2
N K	49.3	43.3
Si K	0.8	0.3

expected, both the flexural strength and fracture toughness decreased evidently with increasing PMMA content.

For porous Si_3N_4-based ceramics, the mechanical properties are closely related to their microstructure, especially the porosity and β-Si_3N_4 grain morphology. Many studies [6, 22, 23] indicated that high fracture toughness is attributed to the elongated β-Si_3N_4 grains, which favor crack bridging and deflection; and increasing porosity is detrimental to the flexural strength and fracture toughness. According to the SEM analysis of the porous BN/Si_3N_4 ceramics, α- to β-Si_3N_4 transformation and growth of β-Si_3N_4 grain were greatly blocked due to the introduction of BN and PMMA. Finally, porous BN/Si_3N_4 ceramics with high porosity, low β-Si_3N_4 content, and low aspect ratio β-Si_3N_4 grains were obtained in this study. Therefore, the flexural strength and fracture toughness decreased with increasing PMMA content as indicated in Fig. 4 can be well understood based on above explanations.

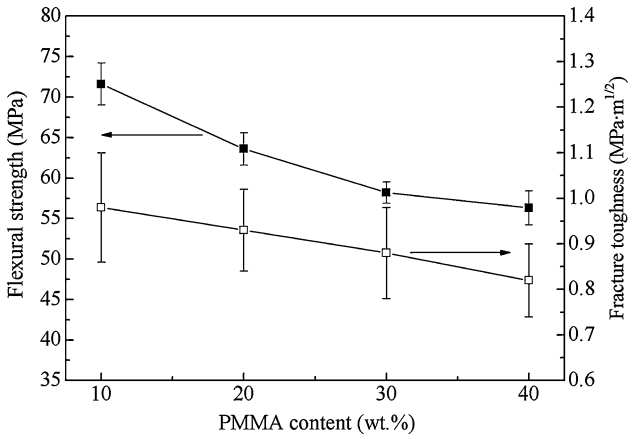

Fig. 4 Effect of the content of PMMA on flexural strength and fracture toughness of the porous BN/Si_3N_4 ceramics

In order to evaluate the thermal stress crack initiation of ceramic materials, thermal stress fracture resistance parameter R, which is also known as thermal shock critical temperature difference (ΔT_C) introduced by Kingery [24] to estimate thermal stress fracture resistance of ceramic materials:

$$R = \Delta T_C = \frac{\sigma_f(1-v)}{\alpha E} \quad (2)$$

where σ_f is the flexural strength, v is the Poisson ratio (suppose to be 0.26 for all the samples [25]), E is the Young's modulus, α is the coefficient of thermal expansion.

The ΔT_C was calculated based on the measured Young's modulus and thermal expansion coefficient, as shown in Table 3. It can be found that ΔT_C value of the obtained samples increased evidently with increasing PMMA content. According to Fig. 4 and Table 3, we found that the

Table 3 Thermal expansion coefficients and the calculated values of critical temperature difference of the porous BN/Si_3N_4 ceramics

Designations	Young's modulus (GPa)	Thermal expansion coefficient (10^{-6} K^{-1})	Critical thermal shock temperature difference (°C)
P10	25.04 ± 2.17	3.07	688.7
P20	21.96 ± 2.01	2.95	726.0
P30	13.75 ± 1.40	2.93	1067.2
P40	11.78 ± 0.75	2.92	1209.0

increasing of PMMA content caused a moderate decrease of flexural strength while the Young's modulus declined rapidly, and the coefficient of thermal expansion, which depends entirely on the type of bonds present in the material and is not affected by the presence of porosity, almost unchanged for all of the four samples. The combined results of the three factors account for the improvement of ΔT_C value. In addition, the porous ceramics with connected open pore structures also present good thermal shock resistance, because the pores can promote the reduction of stress concentration during the quenching process [26, 27].

Dielectric properties of the porous BN/Si_3N_4 ceramics

The microstructure features (porosity, phase composition, pore structure, etc.) that influence mechanical properties of ceramics also influence electrical properties. The effects of these elements on dielectric constant (ε) could be characterized by mixture law. The porosity decreases the strength of a ceramic, and meanwhile, it also decreases the constant (ε) and dielectric loss tangent (tanδ). ε and tanδ of pores can be regarded as 1 and 0, separately, and the variation of ε with porosity can be considered by using an approximation as Eq. (3) based on mixture law [28]:

$$\varepsilon = \varepsilon_0 - P\,(\varepsilon_0 - 1) \tag{3}$$

where ε_0 is the dielectric constant of ceramic matrix, and P is the porosity. It can be seen that the dielectric constant of porous ceramic decreases obviously with increase in porosity. Compared to β-Si_3N_4, α-Si_3N_4 ceramic shows better dielectric properties, whose ε is 5.6 and tanδ is 0.003 at room temperature than that of β-Si_3N_4 ceramic ($\varepsilon = 7.9$, tan$\delta = 0.005$). What's more, the micro spherical-shaped pores homogeneously distributed in ceramic matrix can avoid many sharp edges. The sharp edges may cause more reflections in the ceramics and low permeate flux through the samples and result in increased ε and tanδ [14, 17].

Figure 5 shows (a) the relationship between dielectric constant, (b) dielectric tangent loss and frequency (at the range of 21–33 GHz) of the porous BN/Si_3N_4 ceramics

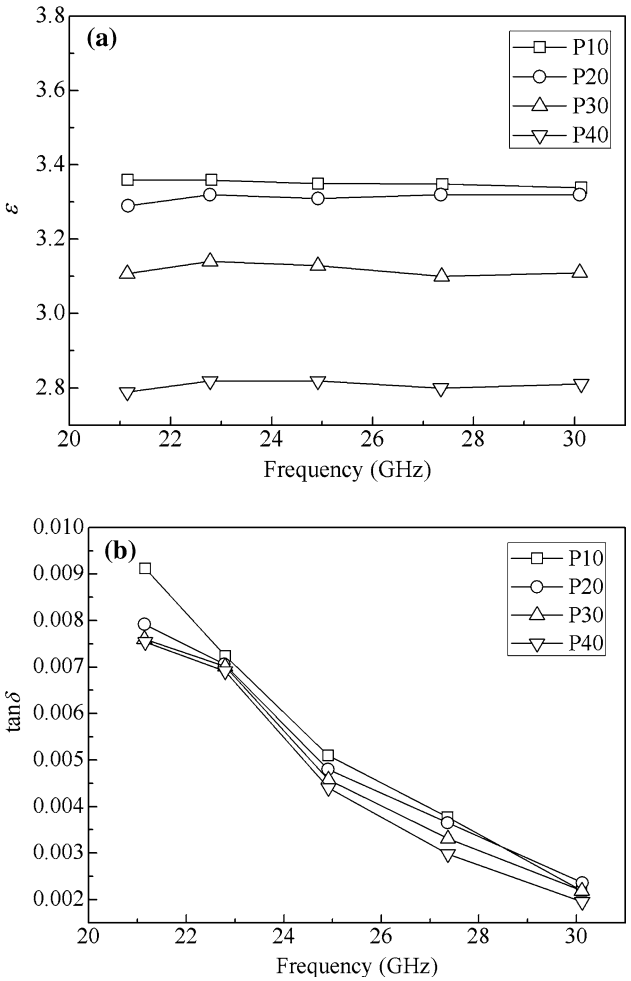

Fig. 5 **a** Dielectric constant and **b** dielectric loss tangent of pores BN/Si_3N_4 ceramics depending on the content of PMMA

with different PMMA content, respectively. It can be found that ε and tanδ of the as-prepared samples increased evidently with increase in PMMA content. High porosity, α-Si_3N_4 content, and the spherical-shaped pores in the porous BN/Si_3N_4 ceramics are all contributed to decrease the ε and tanδ values.

Conclusions

Porous BN/Si_3N_4 ceramic has been prepared by gel casting using a fugitive, PMMA, and samples have been produced with volume fractions of porosity from 53 to 61 %. Finally, porosity, P, was controlled as a function of the PMMA content.

The microstructure of the ceramics shows bimodal hierarchical structures composed of spherical-shaped micro pores depending on starting PMMA content and sub-micro pores formed by stacking ceramic particles. The micro pores uniformly dispersed in the ceramic matrix, and the

sub-micro pores are acted as channels between micro pores. α to β transformation of Si_3N_4 and the growth of β-Si_3N_4 grain was restrained by the BN scattered between β-Si_3N_4 grains, as well as aggregated on the wall of micro pores. Furthermore, mechanical and dielectric properties of the obtained porous ceramics that rely on porosity can be well adjusted by the starting PMMA content. The overall performance of the obtained porous BN/Si_3N_4 ceramic with excellent dielectric properties, good thermal shock resistance, and moderate mechanical properties indicates that it could be one of the most ideal candidates for high-temperature applications.

Acknowledgements This work was supported by Yangtze Scholars Program in China (2009); National Natural Science Foundation of China (NSFC, 51021002, 51225203).

References

1. Krstic Z, Krstic VD (2012) J Mater Sci 47:535. doi:10.1007/s10853-011-5942-5
2. Li YL, Li RX, Zhang JX (2008) Mater Sci Eng A 483–484:207
3. Shuba R, Chen IW (2006) J Am Ceram Soc 89:2147
4. Wang SJ, Jia DC, Yang ZH, Duan XM, Tian Z, Zhou Y (2013) Ceram Int 39:4231
5. Xia YF, Zeng YP, Jiang DL (2012) Mater Des 33:98
6. Li SQ, Huang Y, Wang CA, Zan QF, Li CW (2001) J Mater Sci 36:4103. doi:10.1023/A:1017936014726
7. Lienard SY, Kovar D, Moon RJ, Bowman KJ, Halloran JW (2000) J Mater Sci 35:3365. doi:10.1023/A:1004880901978
8. Kawai C (2001) J Mater Sci 36:5713. doi:10.1023/A:1012542421983
9. Díaz A, Hampshire S (2004) J Eur Ceram Soc 24:413
10. Kawai C, Matsuura T, Yamakawa A (1999) J Mater Sci 34:893. doi:10.1023/A:1004532200735
11. Mao XJ, Wang SW, Shimai S (2008) Ceram Int 34:107
12. Zhang RB, Fang DN, Pei YM, Zhou LC (2012) Ceram Int 38:4373
13. Zhang W, Wang HJ, Jin ZH (2005) Mater Lett 59:250
14. Li SQ, Pei YC, Yu CQ, Li JL (2009) Ceram Int 35:1851
15. Ye F, Zhang JY, Zhang HJ, Liu LM (2010) J Alloys Compd 506:423
16. Wang HJ, Yu JL, Zhang J, Zhang DH (2010) J Mater Sci 45:3671. doi:10.1007/s10853-010-4412-9
17. Li FS, Zhou WC, Hu HJ, Luo F, Zhu DM (2009) Ceram Int 35:3169
18. Gain AK, Song HY, Lee BT (2006) Scripta Mater 54:2081
19. Shao YF, Jia DC, Zhou Y, Liu BY (2008) J Am Ceram Soc 91:3781
20. Meille S, Lombardi M, Chevalier J, Montanaro L (2012) J Eur Ceram Soc 32:3959
21. Ryshkewitch E (1953) J Am Ceram Soc 36:65
22. Large FF (1979) J Am Ceram Soc 62:428
23. Yang JF, Shan SY, Janssen R, Schneider G, Ohji T, Kanzaki S (2005) Acta Mater 53:2981
24. Kingery WD (1995) J Am Ceram Soc 38:3
25. She JH, Yang JF, Ohji T (2003) J Mater Sci Lett 22:331
26. Inagaki Y, Ohgi T (2000) J Am Ceram Soc 83:1807
27. Sudhakar Reddy E, Noudem JG (2007) Energ Covers Manage 48:1251
28. Penn SJ, Alford NM, Templeton A (1997) J Am Ceram Soc 80:1885